Note: Snapshot PDF is the proof copy of corrections marked in EditGenie, the layout would be different from typeset PDF and EditGenie editing view.

Author Queries & Comments:

Q1 : Please note that the ORCID section has/have been created from information provided through CATS. Please correct if this is inaccurate.

Response: Resolved

Q2 : Please check whether "figure 3 citation have been set correctly.

Response: Resolved

Q3 : The disclosure statement has been inserted. Please correct if this is inaccurate.

Response: Resolved

Q4 : Funding details ("HyPOWERED") have been taken from information supplied with your manuscript submission and checked against the Open Funder Registry and we failed to find a match. Please check and resupply the funding details if necessary.

Response: Resolved

Q5 : Funding details (Ministry of University and Research) have been taken from information supplied with your manuscript submission and checked against the Open Funder Registry and we failed to find a match. Please check and resupply the funding details.

Response: Resolved

Q6 : Please note that the Funding section has been created by summarising information given in your acknowledgements. Please correct if this is inaccurate.

Response: Resolved

Q7 : The CrossRef database (www.crossref.org/) has been used to validate the references. Mismatches between the original manuscript and CrossRef are tracked in red font. Please provide a revision if the change is incorrect. Do not comment on correct changes

Response: Resolved

Q8 : Please provide missing city for reference [37].

Response: Resolved

Q9 : Please provide missing city for reference [42].

Response: Resolved

Q10 : Please provide missing city for reference [43].

Response: Resolved

Q11 : Please provide missing city for reference [44].

Response: Resolved

Effect of slit pattern on the structure of premixed flames issuing from perforated burners in domestic condensing boilers

Recto running head : *Combustion Theory and Modelling*

Verso running head : *R. Lamioni et al.*

Rachele Lamioni[a], Cristiana Bronzoni[b], Marco[Q1] Folli[b], Leonardo Tognotti[a], Chiara Galletti[a]

[a] Dipartimento di Ingegneria Civile e Industriale, Università di Pisa, Pisa, Italy;

[b] Ricerca & Sviluppo – Laboratorio Sviluppo Prodotti, Immergas S.p.A., Brescello, Italy

Corresponding author. Email: rachele.lamioni@unipi.it

History : received : 2022-2-16 accepted : 2022-12-5

ABSTRACT

Domestic condensing boilers are equipped with perforated burners ensuring short-length premixed flames issues from a series of circular holes and slits. Despite some efforts that have been devoted to understanding the effect of hole diameter, pattern, and hole-to-hole distance on the resulting flames, very little is known about the flames from a series of slits. In this work 3-dimensional numerical simulations with skeletal kinetic mechanisms are performed to determine the structure of premixed methane-air flames issuing from two-slits patterns, often recurring in practical burner designs, i.e. several equally-spaced slits and a group of four slits. The arrangement of the slits greatly influences the resulting flames. A significant change in the flame behaviour occurs depending on the inlet velocity; at low speeds, the flames issuing from the slits present a flat region, while increasing the speed they assume a conical shape along the slit length. Neighbour flames are distinct from each other at low speeds, while they interact strongly with increasing the velocity. Interestingly, a series of several slits produce a single long wedge-shaped flame, while the group of four slits generates a single conical flame.

Keywords

- laminar premixed flame
- laminar flame propagation
- combustion process
- multi-slit
- condensing boilers
- computational fluid dynamics

FUNDING

The present work was supported by the POR FESR 2014–2020 'HyPOWERED[Q4]' project, funded by Regione Emilia-Romagna Italy and by the Ministry of University and Research[Q5] (MUR) as part of the PON 2014–2020 'Research and Innovation' resources – Green/Innovation Action DM MUR 1062/2021.[Q6]

1. Introduction

In the near future, the European natural gas network could undergo significant changes in gas composition because of the increasing integration of renewable energy sources. Indeed, Europe is planning to inject in the network hydrogen produced from excess solar and wind power, replacing 2% by vol. of the natural gas by 2030, with demonstrations up to 20% by vol. being currently underway [1]. Hence, end-user appliances as domestic boilers must be able to face such variations in the fuel composition and ensure optimal performances while limiting the emission of pollutants [2]. The attention is towards condensing premixed boilers, as they will be soon the leading technology because they provide higher energy efficiency with lower emission of pollutants in comparison with non-premixed ones [3].

Modern condensing boilers are usually equipped with cylindrical or flat perforated burners which inject a premixed mixture into the combustion chamber by generating short-length flames and uniform temperature [4]. The flames should be short enough to accommodate compact volumes, as the distance between the heat exchanger and the burner is lower than in conventional boilers. The burner plays a key role, but its design still mainly relies on the manufacturers' experience and trial-and-error procedures [3]. The reason is that, so far, the improvement of the combustion performance has not been an issue [5]. However, the upcoming variations in the gas composition, with the introduction of fuels with reactivity and power densities that may differ significantly from those of natural gas, as well as the more severe regulations on the emission of pollutants, pose new challenges that require a better comprehension of the combustion process in domestic boilers [6].

In this context, the application of mathematical models based on Computational Fluid Dynamics (CFD) is partially hindered by the complexity of premixed flames [7], as well as by the computational cost needed to describe transport, reaction, and heat exchange. Just a few numerical simulations of burners in domestic boilers can be found in literature, and most of them are limited to the mixing problem or simplified computational domains and models. For instance, Zhang et al. [8] employed CFD to optimise the gas mixing system upstream of a flat perforated burner. Similarly, Zhao et al. [9] carried out numerical simulations to determine the optimal position and dimension of the nozzles exiting from the mixing chamber upstream of a cylindrical perforated burner. Saberi Moghaddam et al. [10] used CFD with a simplified kinetic mechanism to investigate a multi-hole flat flame, showing how the presence of a distribution mesh could improve the flow uniformity among the burner holes. Song et al. [11] numerically analysed propagating premixed flames in tubes with different thermal and velocity boundary conditions using single-step kinetics mechanism. They studied flame structure, flame extinction and the extinguishing of unstable premixed flames in the presence of flame-wall interactions. McIntosh et al. [12] analysed in detail the anchoring of the flames to the burner using simplified chemistry in unstable conditions. Rocco et al. [13] developed a model to study flame stabilisation from perforated plate. Altay et al. [14, 15] carried out 2-dimensional numerical simulations of laminar premixed methane-air flames mimicking a single hole of a flat perforated burner and taking into account the heat exchange with the burner plate. Their results indicated that such heat exchange plays a key role in the flame morphology; if it is neglected, the issuing flame is conical and anchored near the edge of the plate, while if heat exchange is present a positively curved flame occurs downstream of the plate surface, connecting the adjacent conical flames. Kedia and Ghoniem [16] investigates flame stabilisation conditions leading to the blow-off of a laminar premixed flame anchored downstream of a heat-conducting multi-hole burner using 2-dimensional simulations with detailed kinetics. Jothin et al. [17] performed 3-dimensional simulations of laminar premixed propane-air flames issuing from circular holes of a flat perforated burner, observing how the flame stand-off distance increases with increasing the plate thermal conductivity. Besides, the flame moved downstream of the plate by increasing the hole-to-hole distance. Lee et al. [18] study focussed on the design of a domestic gas-condensing boiler to obtain some valuable information regarding the design, in which the burner and heat exchanger must be arranged compactly within a small combustion chamber, especially in terms of simultaneous reduction of NOx and CO emissions.

Veetil et al. [19] performed numerical simulations of steady laminar premixed methane-air flame issuing from circular holes of a flat perforated plate, to investigate the effect hole configuration and hole-to-hole distance on the flame structure. The authors observed the staggered arrangement of the holes to provide higher flame height than the inline arrangement.

Recently, Hinrichs et al. [20] developed a numerical model of a flame issuing from a single circular hole, emulating a portion of a cylindrical perforated burner, and adding a simplified region mimicking the presence of the heat exchange. The model allowed us to gain insight into the chemical pathways to CO and NO in condensing boilers. More specifically CO quickly reaches the equilibrium concentration in the post-flame region; however, the subsequent cooling decreases CO due to oxidation to CO_2 however these oxidation reactions are quickly quenched by the fast depletion of OH radicals. As for NO, a significant contribution of the NNH pathways was observed. redRecently Lamioni et al. [21] have investigated the effect of hydrogen content on multi-hole flames that emulate a portion of burner, which typically use in domestic condensing boilers. All the above configurations regard flames issuing from circular holes. Moreover, several experimental works may be found on perforated burners presenting only circular holes (see for example [22, 23]). However, the holes of typical cylindrical burners installed in domestic condensing boilers, may be either circular or rectangular with rounded edges (slits). Both circular holes and slits could be arranged in series, as we can see from the typical patterns of practical burners reported in [3, 20, 24, 25]. It is worth noting that in such burners, the flames issuing from the series of slits probably play a significant role, as the associated flame lengths are usually larger than those of the flames issuing from the circular holes as we can argue from the images in [24, 26].

Very little is known about laminar premixed flames issuing from a series of slits at conditions relevant for domestic boilers and even less about their numerical modelling as well as identification of key parameters. Mallens and de Goey [27, 28] analysed the stabilisation characteristics of laminar methane-air flames on slit and tube burners, while Mallens et al. [29] extended this analysis to a double slit burner, using a one-step kinetic to investigate M-and V-shaped flames. Parmentier et al. [30] performed 2-dimensional simulations to analyse a lamellae burner, observing that the flame holds at the burner for high lamellae temperatures. Some interesting works are available on the acoustic response of slit or multi-slit flames to acoustic waves. For instance, Kornilov et al. [31] carried our experiments and 2-dimensional numerical simulations with simplified kinetics to investigate the response of premixed methane-air flames issuing from a multi-slit burner to acoustic waves, while more recently Steinbacher et al. [32] carried out a comprehensive analysis to compare the acoustic response of a slit flame to those of a Wedge and Bunsen type flames.

The present work intends to develop and carry out 3-dimensional numerical simulations of premixed flames issuing from a series of slits, emulating portions of real burners in domestic condensing boilers. More specifically, we want to analyse and compare two different slit configurations, hence the goal of the paper is twofold. Firstly we want to improve the knowledge and comprehension of laminar premixed flames issuing from a series of slits, at conditions that are relevant for domestic condensing boilers, as on this topic there is a significant lack of information in the literature. Secondly, we propose the use of numerical modelling to aid the development of the burner, whose design so far is mainly based on manufacturers' experience. We believe that the availability of numerical models may help to face the upcoming restrictions on the environmental impact and to implement strategies for the decarbonisation of domestic heating.

2. Numerical model

2.1. Physical model

Three-dimensional numerical simulations of lean methane-air laminar premixed flames were performed using the kinetic mechanism KEE-

Mech [33], which consists of 17 chemical species and 58 reversible reactions. The problem may be described by conservation equations for mass, momentum, energy, and the transport equations for the mass fractions of chemical species in steady-state conditions:

$$\nabla \cdot (\rho \mathbf{v}) = 0$$

$$\nabla \cdot (\rho \mathbf{v}\mathbf{v}) = \nabla p + \nabla \cdot (\bar{\tau})$$

$$\nabla \cdot (\mathbf{v}(\rho E + p)) = \nabla \cdot (k_{eff} \nabla T) + S_h$$

$$(\rho Y_i) + \nabla \cdot (\rho \mathbf{v} Y_i) = -\rho \mathcal{D}_i \nabla^2 Y_i + R_i$$

where $\mathbf{v}$ is velocity, $\bar{\tau}$ is the stress tensor, S_h is the energy source term, including the contribution of radiation, Y_i is the mass fraction of the i-th species and k_{eff} is the effective thermal conductivity. R_i is the net rate of production or destruction of the i-th chemical species by chemical reaction. $\mathcal{D}_i$ is the molecular diffusion coefficient of the i-th chemical species in the mixture. Binary diffusion coefficients are firstly calculated following the kinetic theory and a modification of the Chapman–Enskog formula; then $\mathcal{D}_i$ is obtained by applying Wilke's mixing rule. Radiation is taken into account with the P1 model[34, 35] using the weighted-sum-of-gray-gases model with coefficients from Smith [36] to estimate the spectral properties of the gas media. NO emissions were estimated by including the thermal, prompt and N_2O-intermediate pathways. The thermal formation was modelled from the Zeldovich scheme by assuming a steady-state for the N radical[37], while the O radical was available in the KEE-Mech scheme. The prompt NO formation from methane was estimated from the one-step mechanism proposed by De Soete [38], while the N_2O intermediate from the 2-step scheme of [39] by assuming a steady state for N_2O.

2.2. Computational domain

Two different configurations are analysed by considering the arrangement of slits in perforated burners. Two examples of cylindrical burner designs presenting slits are given in Figure 1. The design of Figure 1(a) exhibits a continuous series of several slits and is reported in the works of [20, 25, 40]. The design of Figure 1(b) can be found in [3] and presents slits that are arranged in groups of four. These two designs will be denoted as A and B, respectively.

Figure 1. Example of cylindrical burner with (a) A and (b) B designs.

(a) (b)

A focus on the pattern of holes and slits for the two designs is reported in Figure 2: here the dashed black line indicates the investigated region, i.e. comprising only the slits. Each slit presents circular corners, has a length L and width $w_s = 0.05L$. The edge-to-edge distance between two neighbour slits is $d_w = 0.16L$. The computational domain for the first configuration, i.e. A, consists of just a quarter of a slit, because of the geometrical symmetries, and it is indicated with a red dotted line in Figure 2(a). The domain for the second configuration, i.e. B, comprises two half slits and it is illustrated again with a red dotted line in Figure 2(b). Taking advantage of the symmetries at the lateral surfaces of the computational domains, the two domains mimics a series of several equally-spaced slits (see the region delimited by the black dashed line in Figure 2(a)) and a group of four slits (black dashed line in Figure 2(b)), respectively. The distance between the groups of holes and slits is enough to prevent any interaction between the flames issuing from them; hence, the group of slits can be studied alone, i.e. without taking into account the presence of holes. This will enable us to greatly limit the computational cost. However, to better verify this assumption and the adequacy of investigating just the slits, we carried out additional numerical simulations by using a computational domain encompassing both slits and holes. Details on the model and corresponding results are reported in the Appendix A. There we can observe that the predicted flame morphology using just the slits and the one from the complete domain, i.e. with hole and slits, are well in accordance with each other. This evidence motivates the choice of the domains depicted in Figure 2.

Figure 2. Sketch of (a) A and (b) B burner designs. Red dotted lines represent the computational domain.

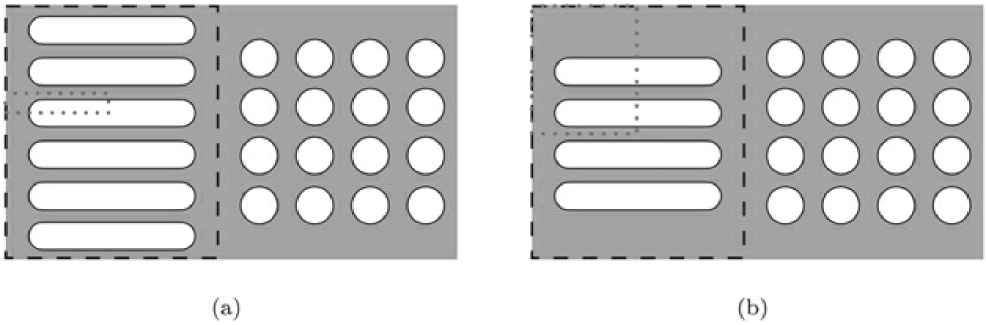

The 3-dimensional view of the computational grids is shown in Figure 3(a,b) **[Q2]**, for the A and B configurations, respectively, along with the reference system of coordinates. It is worth noting that we assume the slits and the plate to be flat. Indeed, even though the burner is cylindrical, such an approximation is sufficiently accurate as the length of the slits is much shorter than the burner perimeter.

Figure 3. Computational grid for (a) A and (b) B configurations.

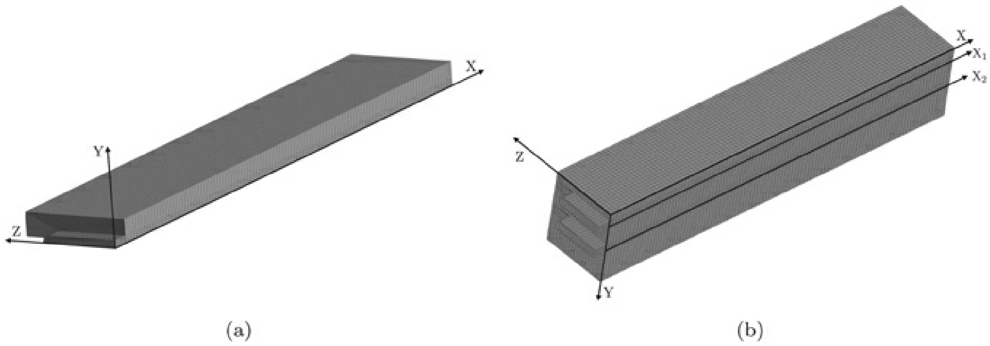

Fully structured grids were created with ICEM by ANSYS Inc., using the O-grid strategy to deal with the round edges of the slits. At least □10 computational nodes were ensured within the thermal flame thickness, which was preliminarily estimated from the 1-dimensional simulation of a freely propagating flame, using the open-source code Open-Smoke-Suite [41]. More specifically, the thermal flame thickness l_T was calculated from the estimated temperature profile of the freely propagating flame across the flame front [42] as:

$$l_T = \frac{T_b - T_u}{\frac{\partial T}{\partial x}\Big|_{\max}}$$

where T_b and T_u are temperatures of the burnt and fresh gases, respectively and $\partial T/\partial x$ is the temperature gradient.

2.3. Grid independence

A grid independence study was carried out for the A configuration, confirming the suitability of the chosen cell size in the flame front. For this configuration, a grid convergence study was performed using the Richardson extrapolation method. Figure 4 shows the temperature and the OH mole fraction profiles along the slit axes for three different grids, namely fine, medium and coarse. In this work, the medium grid (89k cells) is chosen considering the Grid Convergence Index (GCI) value between the medium and the fine mesh less than 2%. For the B configuration, the grid was built on this basis, i.e. by using the same number of nodes for the same characteristic lengths as for the A configuration. The extension of the computational domains referred to the slit length, i.e. L, and the corresponding number of computational cells are summarised in Table 1 for both A and B configurations. A $_1$, A $_2$ and A $_3$, refer to case A with increasing values of the flow rate.

While the same computational domain was retained for the A_1 and A_2 cases, the length of the domain was doubled for the highest flow rate, i.e. for the A_3 case, to avoid the flame exceeding the domain. Same considerations hold for B_1, B_2 and B_3 cases.

Figure 4. Grid convergence for A configuration for (a) temperature and (b) OH profiles along the slit axis.

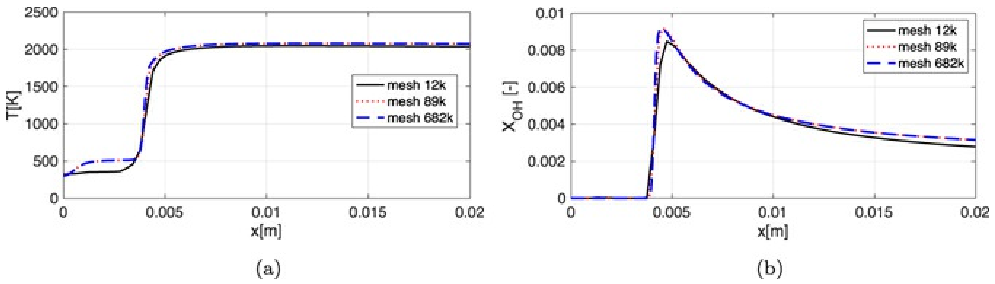

Table 1. Dimension of the computational domain and number of computational cells for the different test cases.

Case	Domain	N_2cell
A_1-A_2	$4L \times 0.68L \times 0.15L$	89000
A_3	$8L \times 0.68L \times 0.15L$	177000
B_1-B_2	$4L \times 0.68L \times 0.75L$	310000
B_3	$8L \times 0.68L \times 0.75L$	500000

2.4. Boundary conditions

The boundary conditions were determined by analysing the thermal power of three experimental tests that were available for a condensing boiler equipped with a burner of B design. In particular, the outlet NOx emissions were measured for a thermal power corresponding to 15%, 50% and 100 % of the nominal load. The fuel is methane and the equivalence ratio of the mixture is ϕ = 0.8.

Then, the issuing velocity could be determined from the thermal power and equivalence ratio by considering the total area of the burner holes. The estimated velocity values for increasing thermal loads were $v_1 = 3.2S_L$, $v_2 = 8.4S_L$ and $v_3 = 18.8S_L$, where S_L is the laminar velocity of the 1-dimensional freely propagating flame. We remark that the above conditions ensure a fully laminar flow. Uniform velocity, temperature (of 300 K), and composition were set at the entrance of the slits. Pressure outlet condition was given at the exit of the domain, while symmetry conditions were prescribed at the sides. As for the wall region between the slits, a wall temperature of $T = 750$ K was set. This value was taken from experimental data which were available for the boiler burner; moreover, it is well in agreement with the burner temperature commonly reported in the literature [24, 25].

To evaluate the reliability of the experimental temperature values, preliminary simulations were performed on a simplified geometry using the conjugate heat transfer (CHT) approach, which models both fluid and solid domain. The numerical runs concerned a single-hole geometry that was described in a 2D axisymmetry to limit the computational cost, with a structured grid. Figure 5 shows the temperature field in both solid (marked with a grey line) for two different loads, i.e. 15% and 100% of the nominal one. We observe an uniform temperature in the solid zone with values in good accordance with measured ones (the range is 700–780 K). Hence, to limit the computational cost of the simulation we imposed a uniform temperature at the walls from the experiments, in order to model only the fluid zone.

Figure 5. Temperature field in the fluid and solid domain for the G20 mixture for single-hole geometry with CHT approach for 15% and 100% of nominal load.

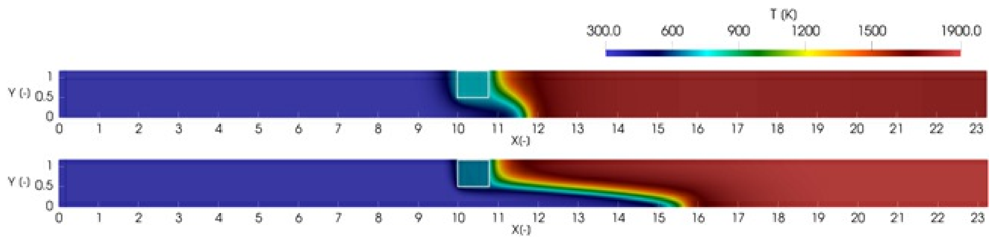

2.5. Solution methodology

The above set of equations was solved with the pressure-based coupled algorithm available in the finite volume code FLUENT 19.2 [43] by ANSYS Inc., using a central differencing scheme for diffusion terms and second-order upwind scheme for convection terms. The computation of the chemistry was carried out through the direct integration method. The fuel-oxidiser mixture was ignited by patching a region near the inlet with a temperature higher than the adiabatic one, i.e. with $T = 2500$ K. At convergence, normalised residuals did not change with iterations and were all below 10^{-6}.

2.6. Verification

To verify the reacting flow module with the detailed chemistry of the computational model, a 3-dimensional flame in A and B configurations is compared with 1-dimensional freely propagating flame simulated using Open-Smoke-Suite code [41]. Simulations were performed using the same methane-air reaction mechanism in both of the cases. Figure 6(a) shows the comparison of the temperature profiles for 3D simulations for A1 and B1 configurations and 1D freely propagating flame. Figure 6(b,c) show the comparison of the OH and CO mole fractions profiles. These figures display that, in the flame region, the results of 3D and 1D simulations are in agreement, which indicates the accuracy of the computational procedure adopted for the present work. The discrepancies for the OH mole fraction in the burnt region for configuration B are attributed to the flame interaction. This point will be discussed in the results section.

Figure 6. Comparison of temperature (a) and OH (b) and CO (c) mole fractions profiles of 3D simulation (A1 and B1) results and 1D freely propagating flame.

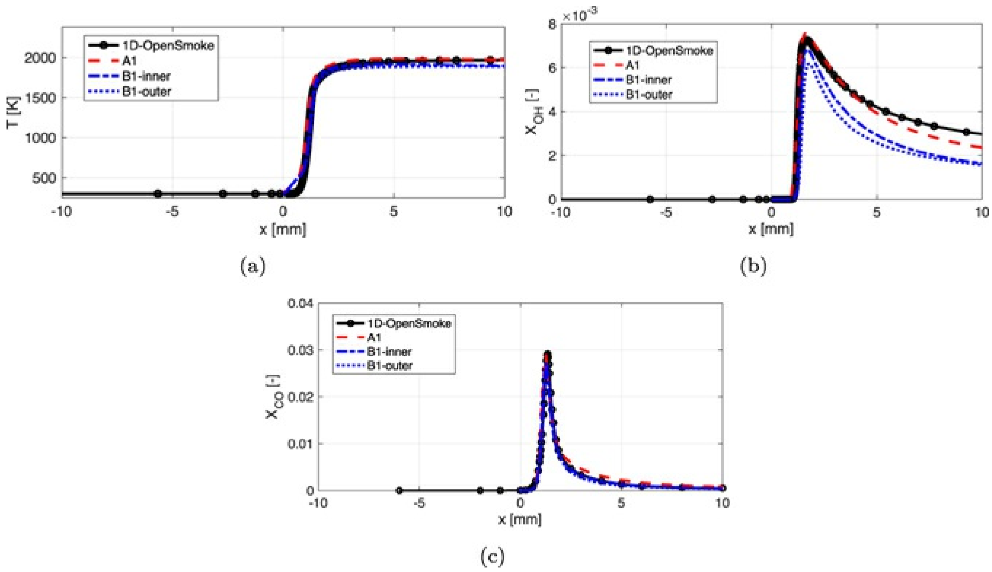

3. Results

The effect of the two configurations on the issuing flame is described in the following text by analysing the thermal and flow fields. In addition, the distribution of the OH radical is provided, as it acts as a flame marker.

Figure 7(a,b) show the temperature field estimated for the two configurations with the lowest inlet velocity, i.e. for A_1 and B_1 cases, respectively. The goal of this figure is to highlight the different arrangements of the slits in the two configurations, thus facilitating the description of the flame structures in the following sections. To this purpose, the temperature field has been reflected here by using the domain symmetries.

Figure 7. Temperature field for for (a) A_1 and (b) B_1 cases.

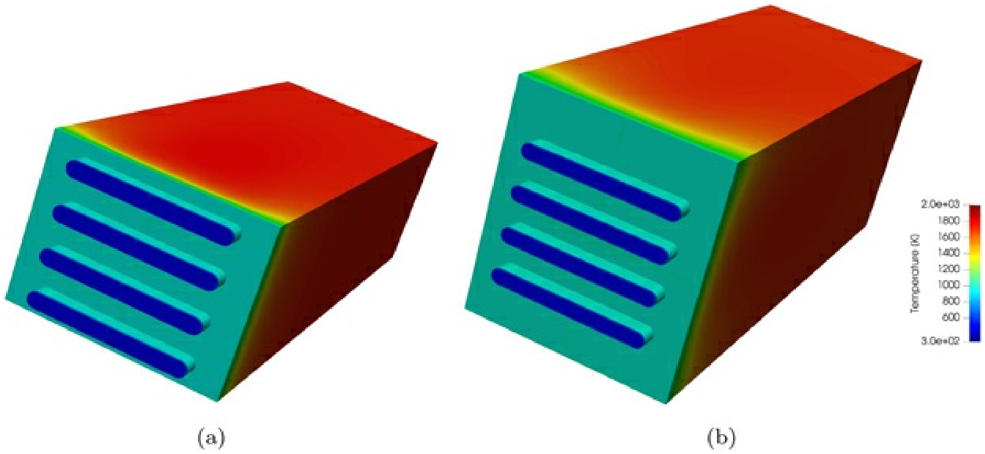

3.1. A configuration

Figure 8 reports the distribution of temperature, OH mole fraction and velocity on the *XZ* and *XY* planes (see Figure 3) for the A design with the lowest inlet velocity, i.e. A_1 case. We can notice from the temperature field in the *XZ* plane that the flame exhibits a flat region near the axis (i.e. towards $Z = 0$) and a lateral curved zone. Indeed, such a low flow rate generates a flame that remains pretty close to the inlet, as we can observe from the OH field in Figure 8(a). The *XY* view indicates that the flame tends to close laterally towards the burner plate, thus indicating that in the multi-slit configuration the flames are well separated from each other.

Figure 8. (a)Temperature, (b) OH mole fraction and (c) velocity fields with streamlines on the *XZ* and *XY* planes for A_1 case.

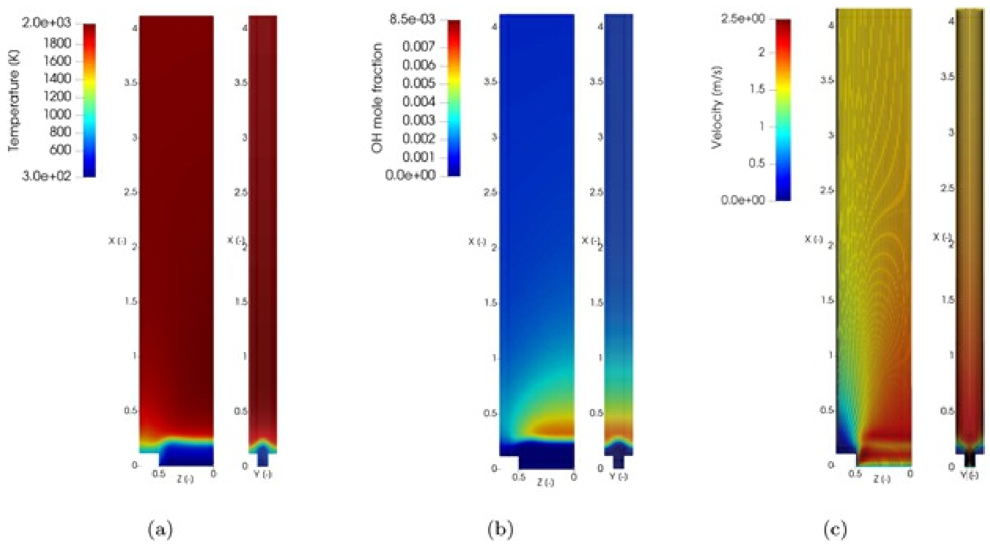

As for the flow field (see Figure 8(c)), we can notice the first increase of velocity very close to the injection, due to the heating up due to the exchange with the burner wall that diminishes the gas density, and then the subsequent acceleration in correspondence of the flame front.

Similarly, Figure 9 shows results for higher inlet flow rate, i.e. for A_2 case. A change in flame morphology concerning the previous A_1 case is well evident, with the flame front moving away from the entrance and assuming in the *XZ* plane, the typical conical structure of a Bunsen flame [44]. The velocity distribution indicates the high-velocity region, near the inlet, triggered by the heating due to the exchange with the burner walls, and subsequently the strong acceleration at the flame tip [45]. We can also observe from the flow streamlines (Figure 9(c)), the presence of a recirculating region just above the burner plate, which is induced by the strong momentum of the inlet jet. The thermal and OH fields in the *XY* show how the flame is unable to attach to the burner plate, hence indicating that neighbour flames merge with each other.

Figure 9. (a) Temperature, (b) OH mole fraction and (c) velocity fields with streamlines on the *XZ* and *XY* planes for A_2 case.

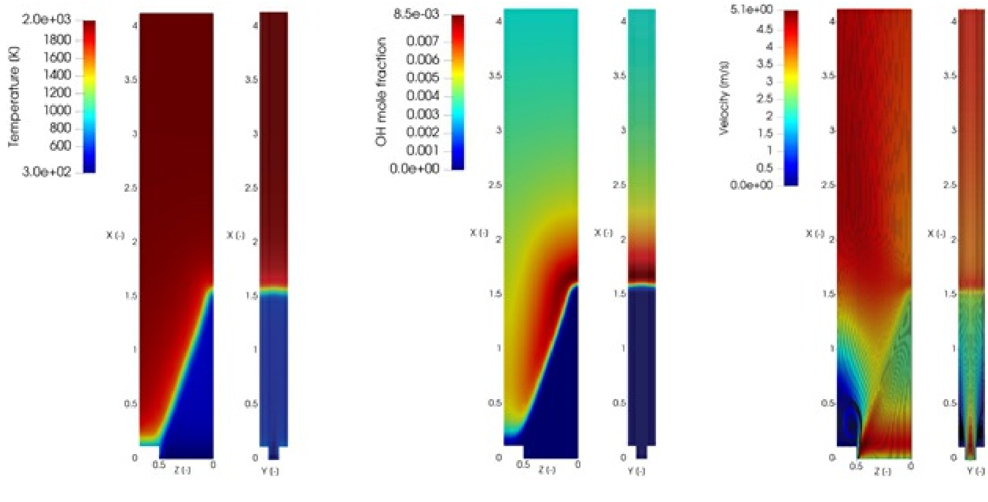

Further increasing the flow rate, i.e. A_3 case in Figure 10, the flame lengthens while maintaining the Bunsen configuration, when looking at the *XZ* plane. It is worth noting that the length of the domain, which is twice the one used for A_1 and A_2 cases, allows avoiding the presence of edge effects. The flow streamlines again highlight the presence of a recirculation region which extends more and appears stronger than the one of the A_2 case.

Figure 10. (a)Temperature, (b) OH mole fraction and (c) velocity fields with streamlines on the *XZ* and *XY* planes for A_3 case.

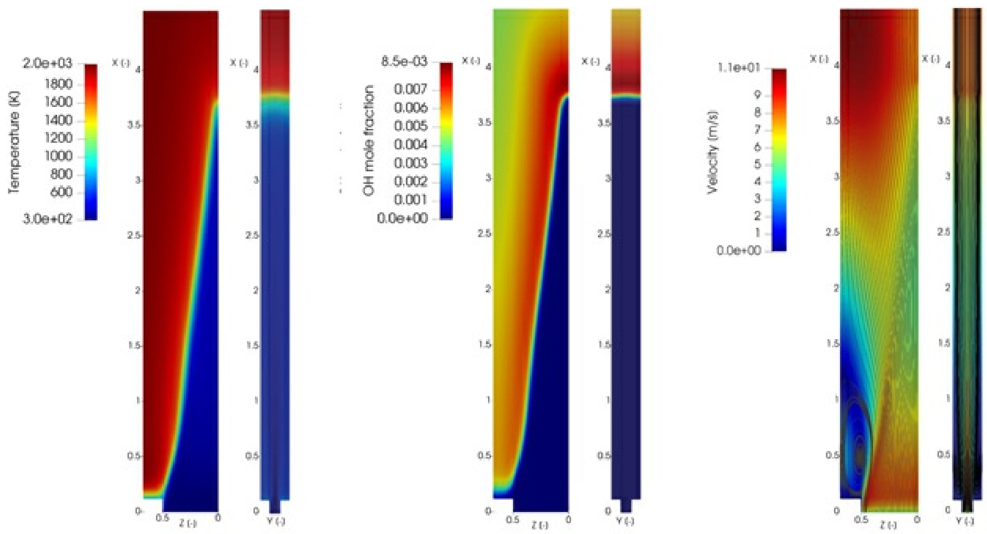

Figure 11(a–c) shows profiles of temperature, OH mole fraction, and velocity along the X axis for A design and all inlet velocities. The axial coordinate $X = 0$ corresponds to the inlet. The velocity values are normalised for the laminar flame speed S_L, calculated from the 1-D freely propagating flame simulations. Temperature profiles confirm that the flame front is well attached to the burner for the lowest velocity, the temperature increase occurring at $X \approx 0.2L$. Augmenting the flow rate, the flame front moves to $X \approx 1.6L$ and $X \approx 3.7L$ for A_2 and A_3, respectively. This is further remarked by the peaks in the OH profiles.

Figure 11. Profiles of (a) temperature, (b) OH mole fraction and (c) axial velocity along the X axis for A design and three inlet velocities.

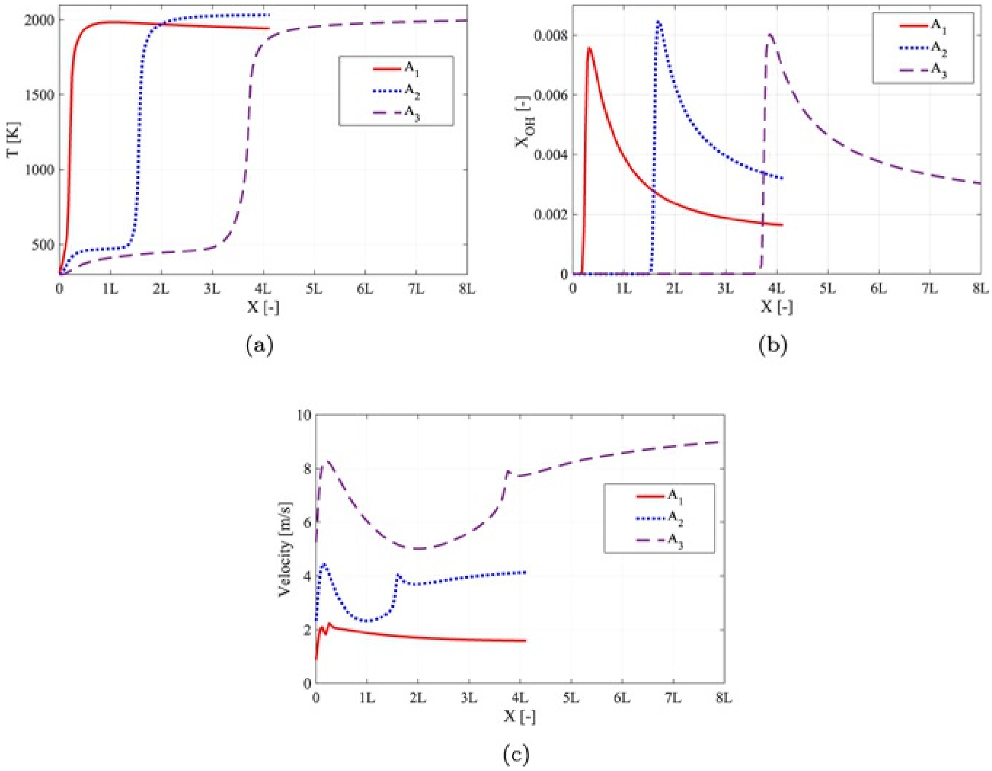

The velocity profiles in Figure 11(c) appear more complex and are characterised by two velocity peaks. The first peak may be explained by the gas acceleration due to the mixture heat up stemming from the heat exchange with the burner; this first peak takes place at $X \approx 0.1L$, with just a slight shift due to the inlet velocity. The second peak occurs just downstream of the flame front, thus its X coordinate increases with the flow rate.

3.2. B configuration

Figure 12(a) reports the temperature distribution for the B configuration and the lowest flow rate, i.e. B_1 case. More specifically three longitudinal views are provided, i.e. XY, X_1Z and X_2Z planes (see Figure 3). The latter two planes cross the inner and outer slits, respectively. We observe that the flames generated by the two slits for the lowest speed value are similar to each other, with a morphology presenting a flat region near the axis and a curved zone. This structure closely follows the one of the A_1 case (see Figure 8). We further notice from the lateral view, that the flame are well distinct, i.e. they do not interact with each other, even though the flame issuing from the outer slit is slightly tilted because of the different extensions of the adjacent hot walls on the left and right sides. This behaviour is further confirmed by the OH distribution in Figure 12(b), which highlights differences between the inner and outer flames. In the latter, the reaction region, marked with OH, is attached on the left, i.e. towards the inner slits, while is lifted on the right side, i.e. towards the burner wall. The streamlines shown in the left panel of Figure 12(c) support the above observations, indicating a tilting of the streamlines exiting from the outer slit. The velocity field in the central and right panels indicates a first acceleration due to the heat up of the inlet gas stream and subsequently a second acceleration at the flame front, as also described for the A_1 case.

Figure 12. (a) Temperature, (b) OH mole fraction and (c) velocity fields with streamlines for B_1 case on (from left to right) the XY, X_1Z (i.e. crossing the inner slit) and X_2Z (i.e. crossing the outer slit) planes.

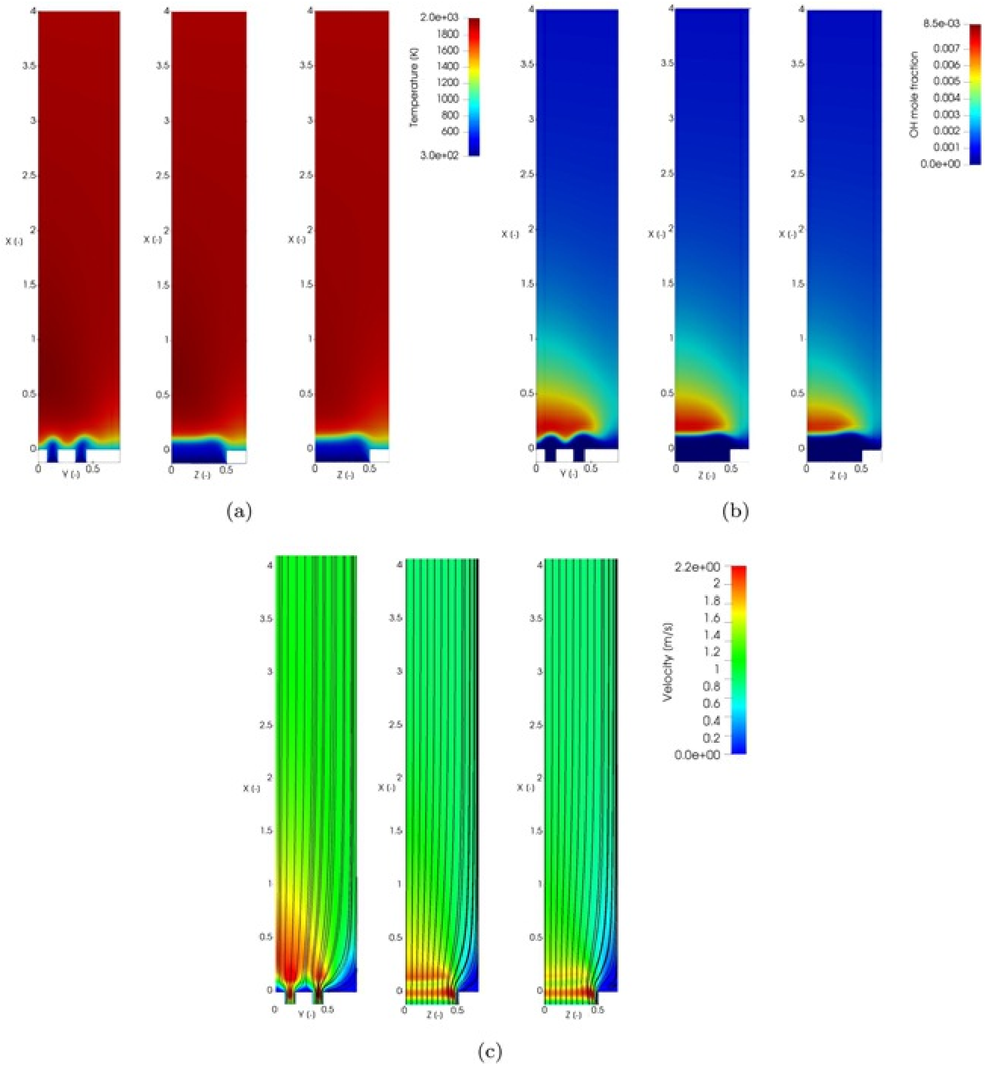

The same fields are shown in Figure 13 for increasing the inlet speed, i.e. for B_2 case. As observed also for the A design, the morphology of the flames is strongly modified with respect to the lowest speed, assuming a conical shape in the XZ plane. However, here we can observe that the flames corresponding to the inner and outer slits differ each other remarkably (see X_1Z and X_2Z planes). In particular, the flame issuing from the outer slit appears closer to the burner, the flame tip being located at $X \approx 0.9L$, than the inner flame, whose tip is at $X \approx 1.4X$. Indeed, the flame of the outer slit is largely affected, on one side, by the presence of the burner wall (see XZ plane), which is hotter than the fresh gases. Therefore, the flame is anticipated with respect to the flame issuing from the inner slit, being surrounded just by cold fresh gases. Moreover, the flame reaction zone (see Figure 13(b)) appears more extended in correspondence of the outer slit with respect to the inner one.

Figure 13. (a) Temperature, (b) OH mole fraction and (c) velocity fields with streamlines for B_2 case on (from left to right) the XY, X_1Z (i.e. crossing the inner slit) and X_2Z (i.e. crossing the outer slit) planes.

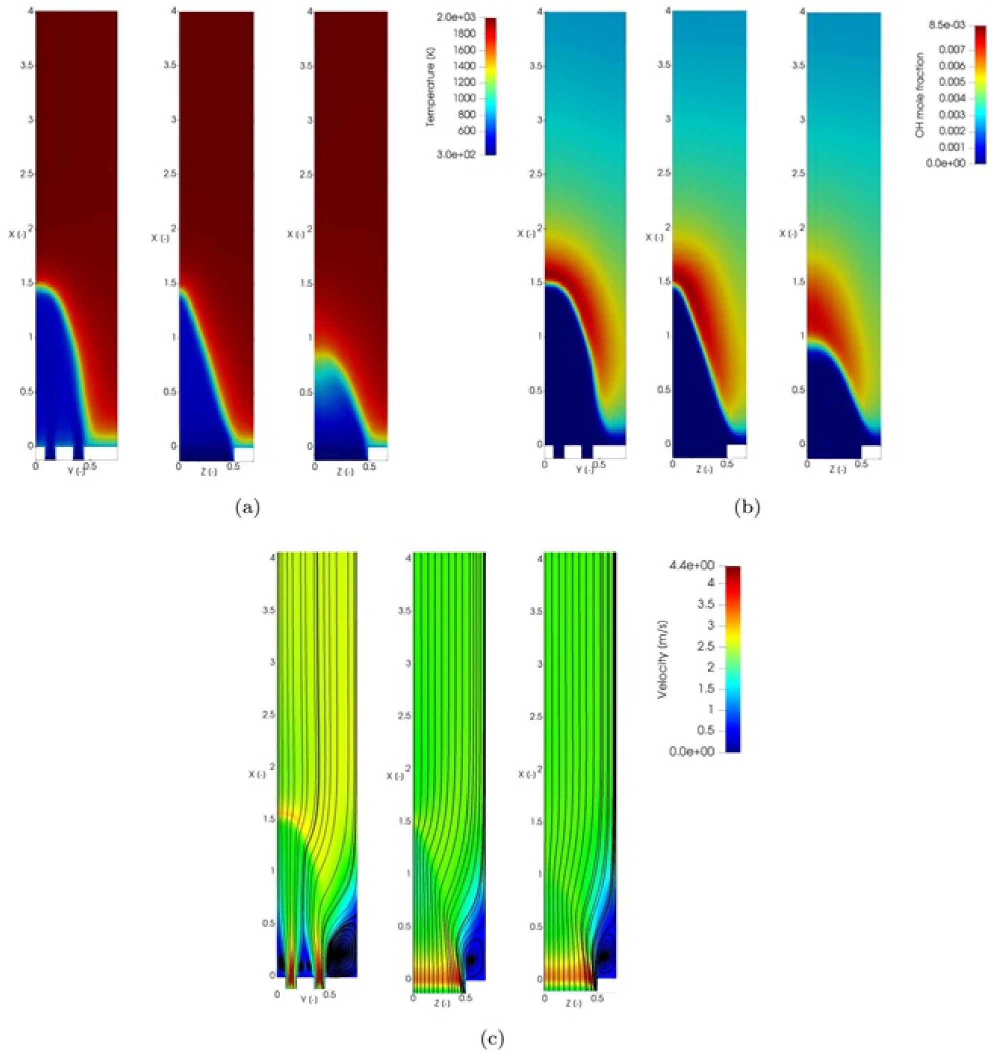

The temperature distribution on the XZ shows just a single flame generated by the flow rates of both slits, rather than two distinct flame fronts anchored to the two nozzles (as for A_1 case). This key feature well denotes a change of flame morphology as the inlet speed increases, with the flames issuing from neighbour slits merging and producing a flame with a larger characteristic length.

The flow field on the left panel of Figure 13(c) clearly shows that the stream from the outer slit is tilted towards the inner one. Besides, a recirculation zone takes place above the burner plate.

Figure 14 reports the temperature, OH and flow fields for the highest speed, i.e. B_3 case, which again exhibits the merging of the flames issuing from the inner and outer slits. The flame tip in correspondence of the inner flame is located at $X \approx 3.6L$ while at $Z \approx 1.8L$ for the outer one. Moreover, we observe a further widening of the reaction zone above the outer slit. The velocity field in Figure 14(c) again reveals the tilting of the stream issuing from the outer slit towards the inlet one, as well as the presence of a strong recirculation region above the wall.

Figure 14. (a) Temperature, (b) OH mole fraction and (c) velocity fields with streamlines for B_3 case on (from left to right) the XY, X_1Z (i.e. crossing the inner slit) and X_2Z (i.e. crossing the outer slit) planes.

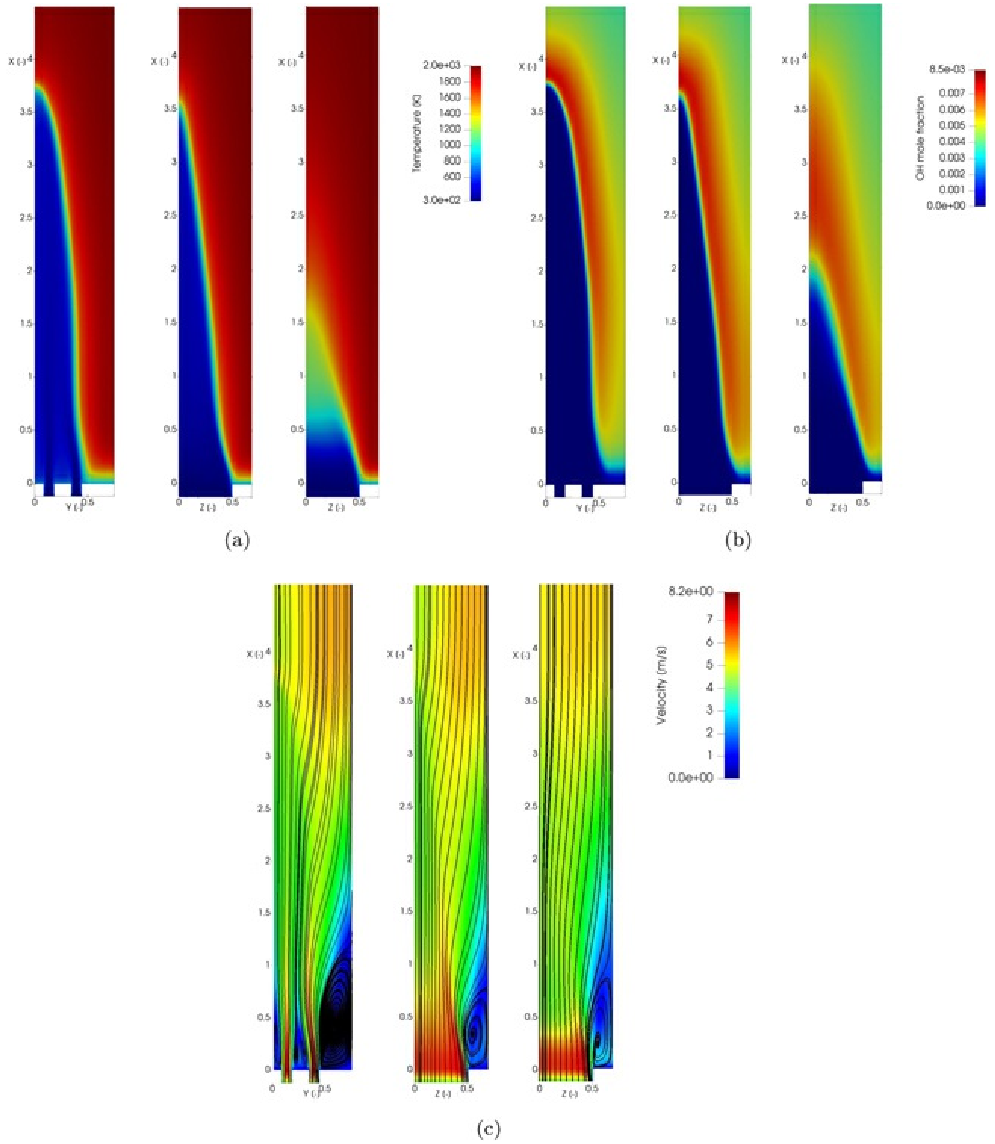

NO emissions for the three thermal loads are available experimentally for the burner shown in Figure 1(b), which presents the B pattern and is installed in a condensing boiler. More specifically, the experimental NOx concentrations were measured using a single-channel multi-gas analyser (nCLD 63, Eco Physics AG, Dürnen, Switzerland). The NO emission values are reported on the dry basis and referring to the same percentage of O_2 to have a quantitative comparison. The experimental NO values are reported in Table 2 along with those predicted for the B configuration. We observe that NO emissions increase with the inlet flow rate, and this is also confirmed by the experimental trend. Besides, the agreement between experiments and CFD is very satisfactory, thus indicating the major role of the flames issuing from the slits in the cylindrical burner as well as the capability of the present numerical model to describe the formation of pollutants.

Table 2. Comparison between experimental NO emissions and those predicted for the B configuration.

Case	predicted NOx [ppm]	experimental NOx [ppm]
B_1	17	13
B_2	20	17
B_3	21	19

3.3. A vs B configuration

The profiles of OH molar fraction along the X axis for A and B configurations are compared in Figure 15 for the three flow rates. For the B configuration, both curves concerning the inner and outer slits are shown, i.e. along the X_1 and X_2 lines. At low inlet velocities (Figure 15(a)), as already discussed, the flames issuing from neighbour slits do not interact. Hence the OH profiles corresponding to the inner and outer slits of the B configuration are similar to each other, with small differences ascribed to the tilting of the outer flame, and pretty alike the A design. This latter configuration shows slightly higher OH values due to the effect of neighbour flames.

Figure 15. Profiles of OH molar fraction along the X axis of A configuration and along X_1 (i.e. inner slit) and X_2 (i.e. outer slit) axes of B configuration at different inlet velocities, i.e.: (a) A_1 and B_1; (b) A_2 and B_2; (c) A_3 and B_3.

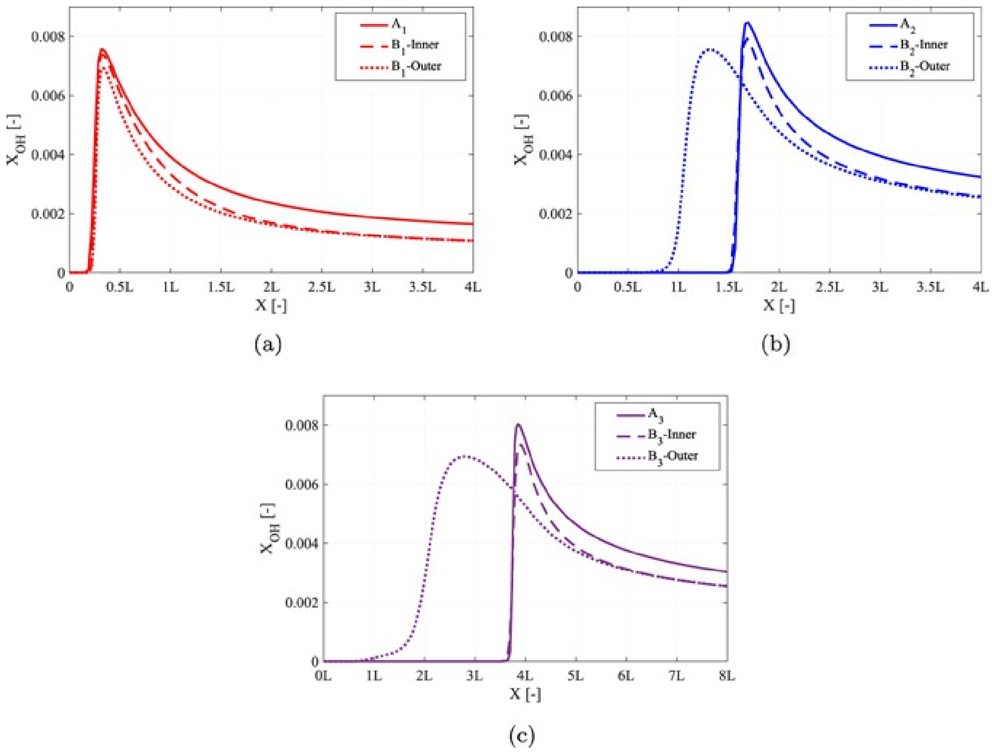

With increasing velocity (Figure 15(b)) profiles for the inner and outer slits of the B configurations deviate each other strongly. The OH peak of the outer slit anticipates and widens to the inner one because of the heating effect given by the burner wall. We can also observe how the profile of the inner slit deviates from the one of the A configuration, thus indicating that an inner slit of a group of four, behaves diffidently than an inner slit of a series of several ones. Similar considerations arise for the highest flow rate (see Figure 15(c)), with the profiles of the inner and outer slits differing remarkably.

The 3-dimensional views of OH iso-contours are shown in Figure16 for the lowest velocity, to better clarify the effect of the slit arrangement on the resulting flames. At low speed, the four flames of the B_1 case are well distinct and pretty alike those of the A_1 arrangement, despite, of course, the already discussed effects near the outer burner walls. With increasing the flow rate, the four slits merge generating a single conical shaped flame in Figures 17(b) and 18(b) for B_2 and B_3 cases, respectively, strongly deviating from the behaviour of an infinite series of slits (see Figures 17(a) and 18(a), respectively) which leads to the presence of a long wedge-shaped flame.

Figure 16. 3-dimensional view of OH mole fraction distribution with iso-surfaces for (a) A_1 and (b) B_1 cases.

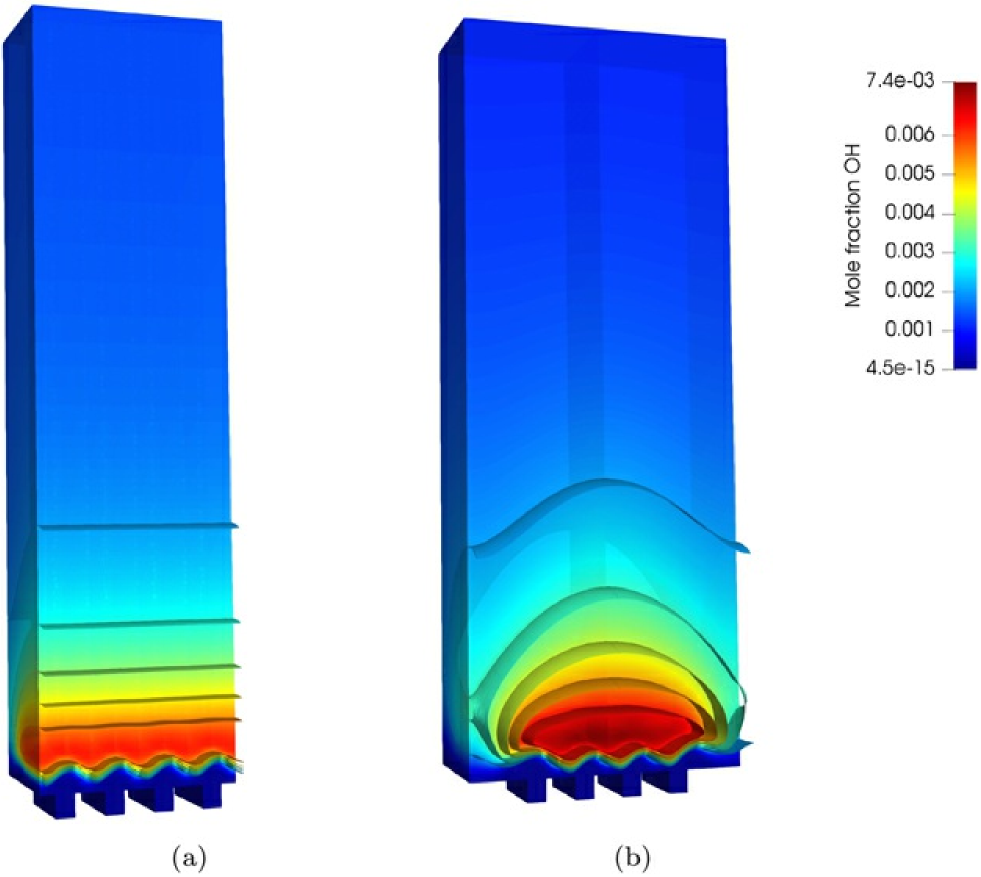

Figure 17. 3-dimensional view of OH mole fraction distribution with iso-surfaces for (a) A_2 and (b) B_2 cases.

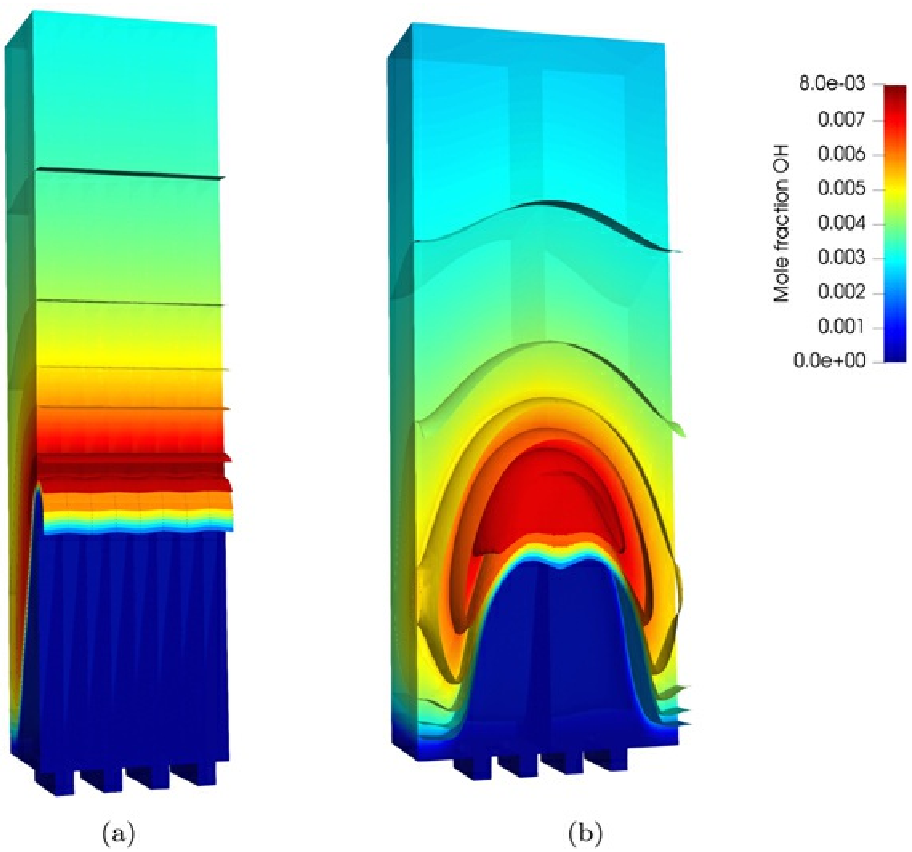

Figure 18. 3-dimensional view of OH mole fraction distribution with iso-surfaces for (a) A_3 and (b) B_3 cases.

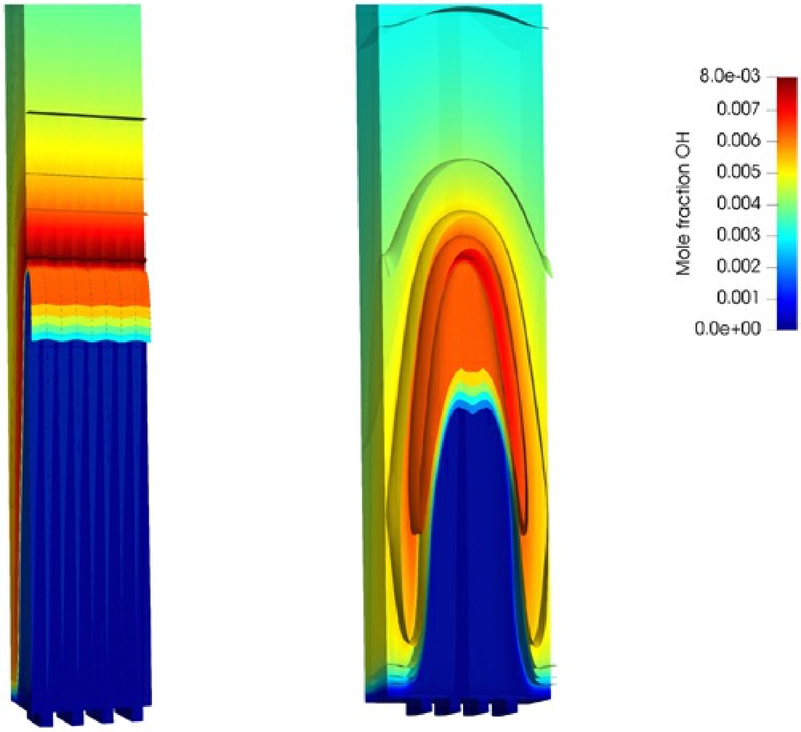

(a) (b)

The temperature profiles for A and B designs along the X axis are compared in Figure 19 for the three velocities. The temperature profile in correspondence of the outer slit well matches those of the inner slit and the A configuration for the low inlet velocity (see Figure 19(a)). Instead, the increase of the flow rate leads to the merging of the flames, whose signature is well evident from the temperature profiles in correspondence of the outer slits (see Figure 19(b,c)).

Figure 19. Profiles of temperature along the X axis of A configuration and along X_1 (i.e. inner slit) and X_2 (i.e. outer slit) axes of B configuration at different inlet velocities, i.e.: (a) A_1 and B_1; (a) A_2 and B_2;(a) A_3 and B_3.

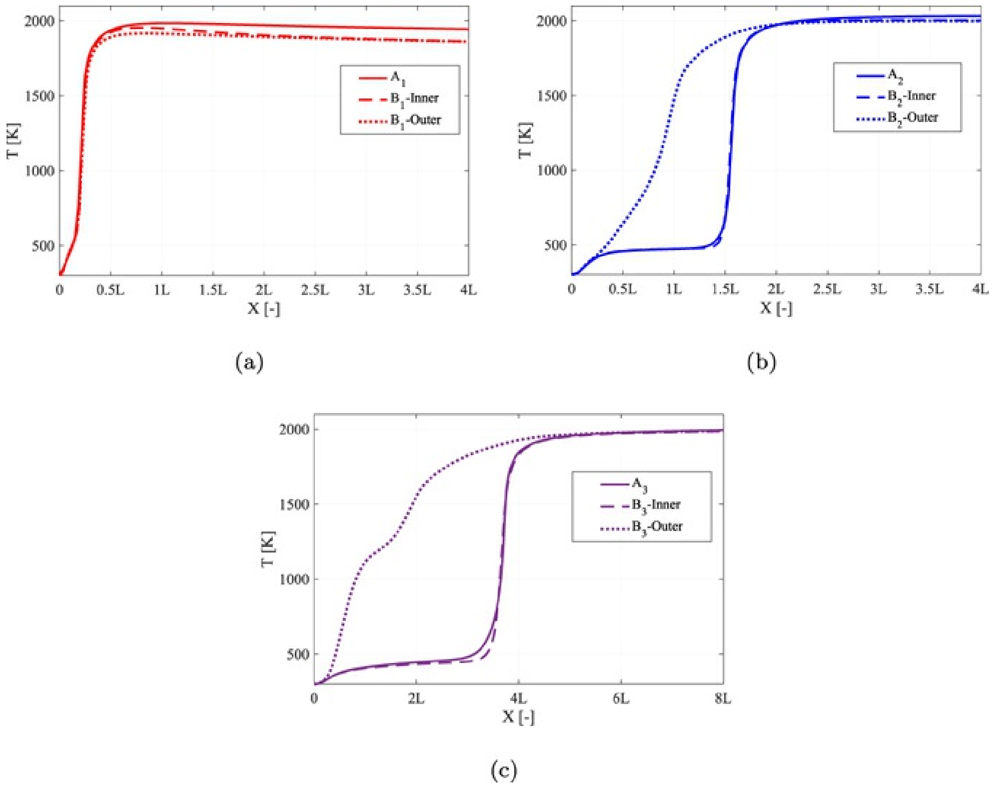

3.4. Numerical simulations with both holes and slits

To verify the adequacy of studying only the slits, because of the large distance between slits and holes, numerical simulations were carried out by using a portion of the burner including both slits and holes. Taking advantage of the pattern symmetries, four half slits, two rows of four half-holes and two rows of entire holes were simulated. The computational grid turned out to be of 2.5 million cells, from a grid independence study, and is shown in Figure 20. Three flow rates, corresponding to 15%, 50% and 100% of nominal power are employed using the KEE-Mech [33] kinetic mechanism.

Figure 20. Computational grid for a burner portion including both slits and holes.

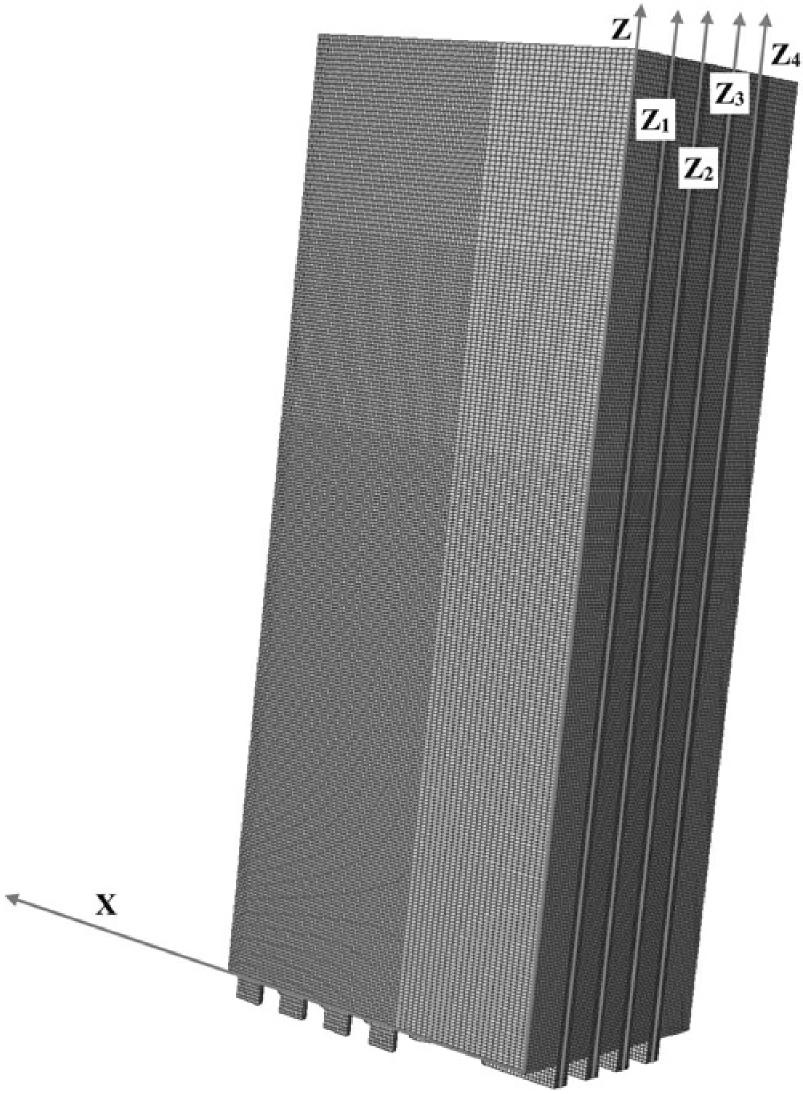

Figure 21 reports the temperature and OH fields for the medium power value. Firstly we can notice how the flames issuing from the slits and the holes are well separated with no interaction. Moreover, the merging of the flames coming out from the inner and outer slits occurs as in the B_2 configuration (see Figure 13(a,b). For a better view, Figure 22 shows the OH distribution along four longitudinal planes. These planes, namely the XZ_1, XZ_2, XZ_3 and XZ_4 planes (see Figure 20), go through the inner and outer slits. We observe that the OH fields are in accordance with the B_2 configuration reported in Figure 13.

Figure 21. Portion of burner: temperature (a) and OH mole fraction (b) fields for 50% of nominal load.

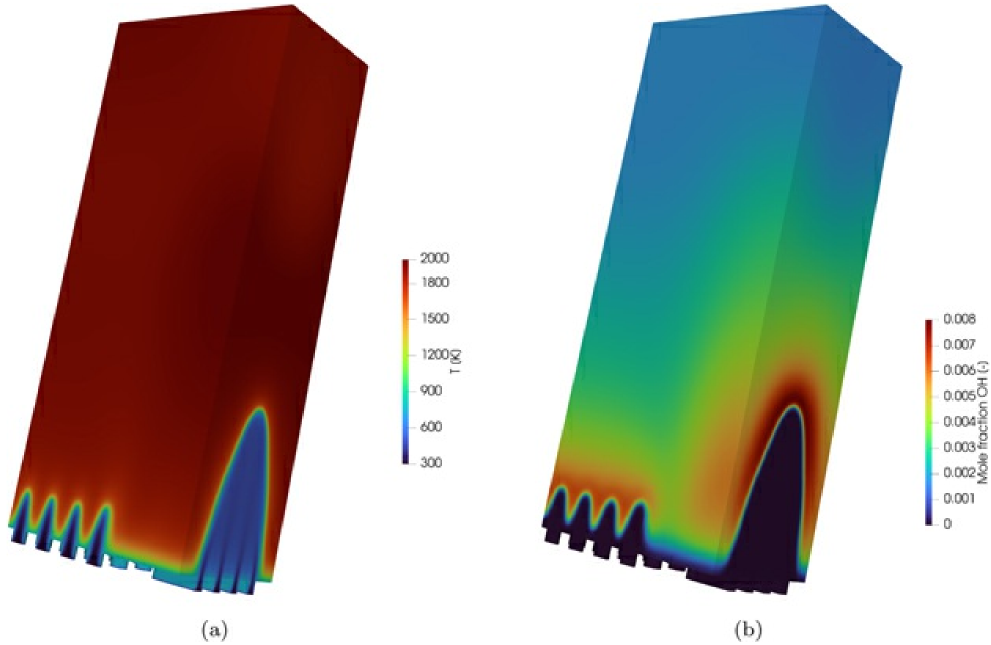

Figure 22. OH field for the burner portion at 50% of nominal load on (from left to right) the XZ_1 (i.e. crossing the outer slit), XZ_2 (i.e. crossing the inner slit), XZ_3 (i.e. crossing the inner slit) and XZ_4 (i.e. crossing the outer slit) planes.

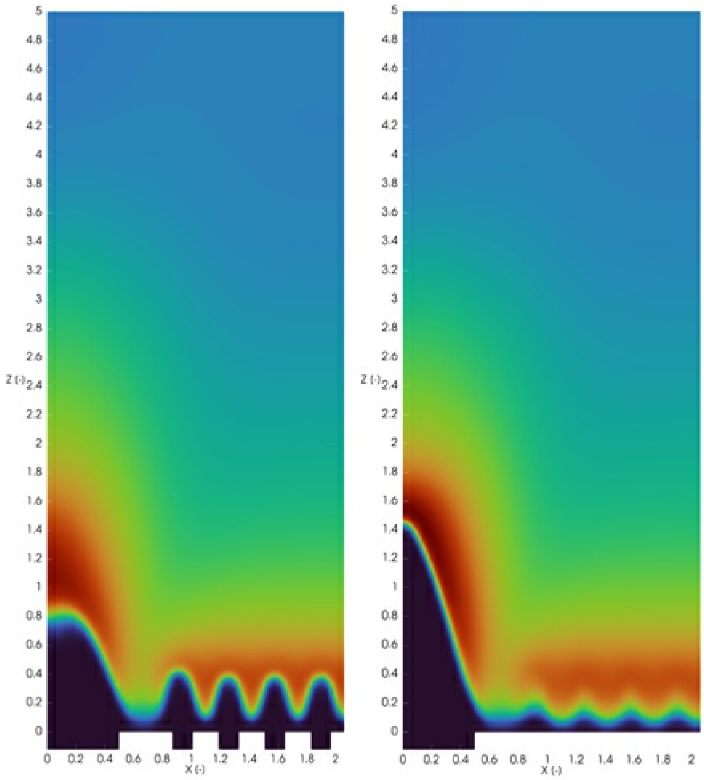

(a)

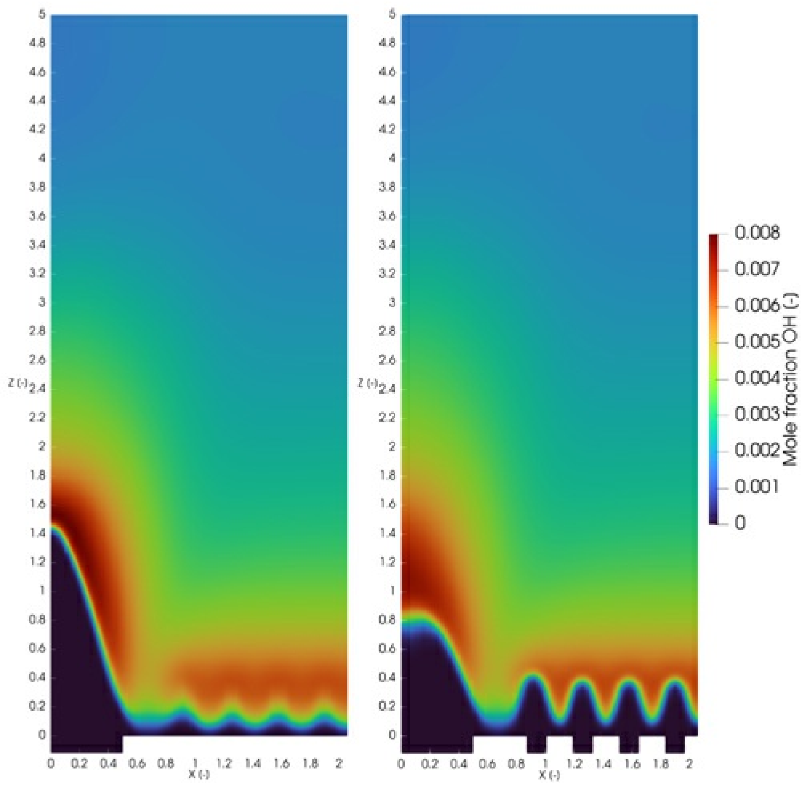

(b)

For a quantitative estimation about the effect of the presence of holes on the flames issuing from the slots, Figure 23 shows the profiles of temperature and OH mole fraction along Z_2 and Z_1 axes predicted with the burner portion compared to the B_2 case. We observe that profiles almost overlaps, thus confirming the suitability of using a reduced domain including only the slits. The same conclusion holds for the other nominal loads, not shown here for sake of conciseness.

Figure 23. Profiles of temperature (a) and OH mole fraction (b) along the Z_2 (i.e. inner slit) and Z_1 (i.e. outer slit) axes for 50% of nominal load.

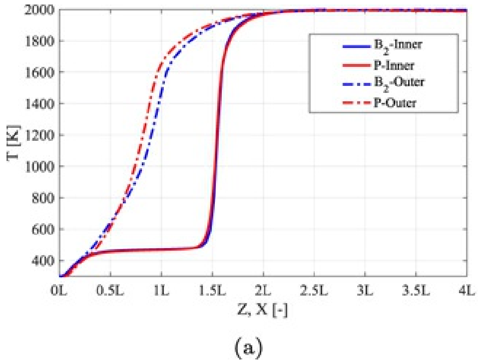

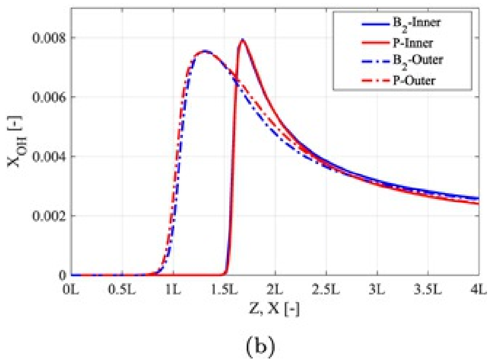

3.5. Effect of H_2 addition on B configuration

A preliminary analysis is made on the effect of H_2 addition by considering the lower nominal power, i.e. 15% of nominal load. We have to stress out that the addition of hydrogen, leads to a change in the equivalence ratio, as better described in details in Lamioni et al. [21]. In particular, when H_2 is added to the fuel mixture, the equivalence ratio naturally decreases, i.e. the excess of air increases. Indeed, the $\phi = 0.8$ for pure natural gas, i.e. 0% H_2 (G20 test gas), shifts to $\phi = 0.74$ for 23% H_2 (G222 test gas) and $\phi = 0.67$ for 50% H_2 (H2NG).

Figure 24 shows the temperature distribution for B_1 configuration for three H_2 contents. It is noted how the morphology of the flames is similar for the three mixtures. Indeed, even though H_2 is characterised by a much larger reactivity than methane, the decrease of the equivalence ration, i.e. increase of dilution, partially hampers this effect. The profiles of temperature along the X axis for B_1 configuration are compared in Figure 25 for the three H_2 content. At this load, as already discussed, the flames issuing from neighbour slits do not interact. Hence the temperature profiles corresponding to the inner and outer slits are similar to each other, with small differences ascribed to the tilting of the outer flame. Increasing the H_2 content the temperature in the burnt zone decreases due to the higher dilution.

Figure 24. Temperature field for G20, G222, H2NG for 15% of nominal load.

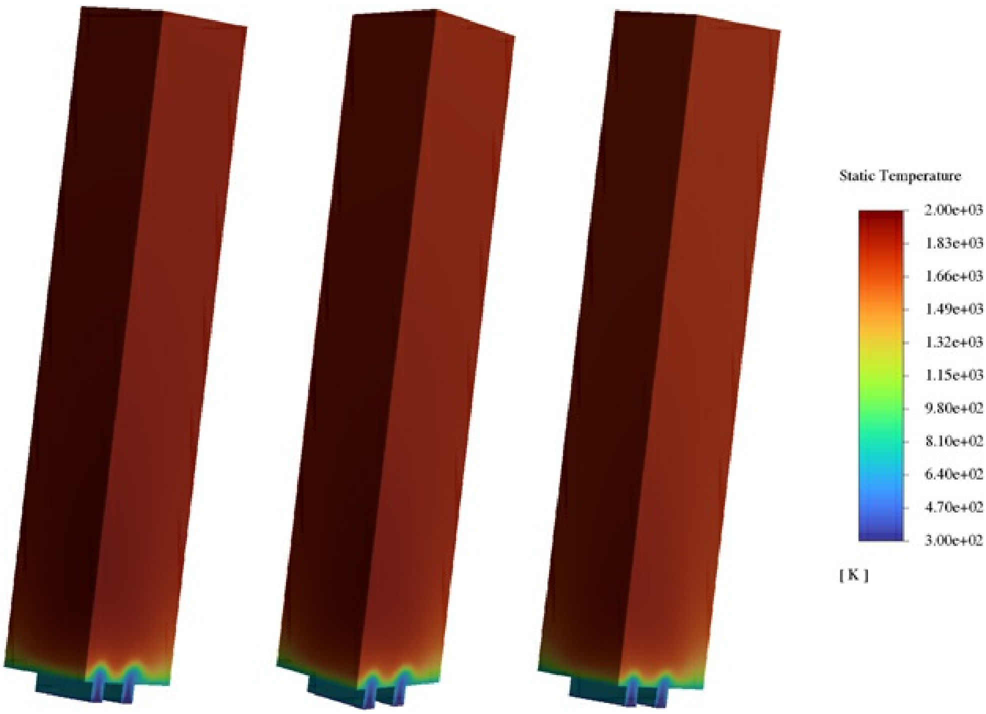

Figure 25. Profiles of temperature along X_1 (i.e. inner slit) and X_2 (i.e. outer slit) axes of B configuration at different H_2 content, i.e.: (a) inner slit; (b) outer slit.

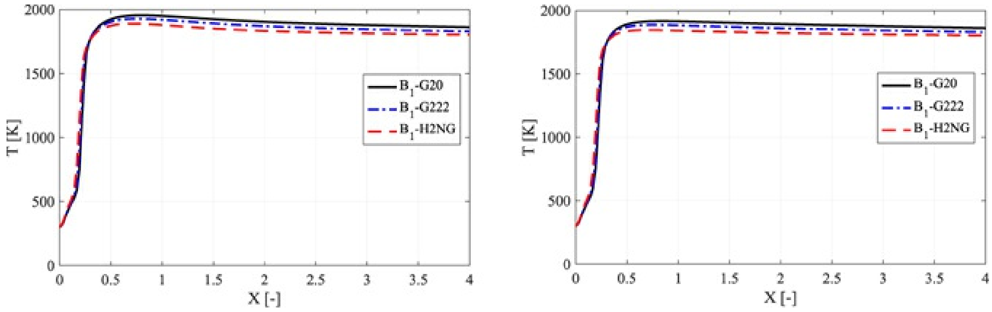

(a) (b)

Figure 26 shows the OH distribution for B_1 configuration at increasing H_2 contents. We see that the flame fronts are similar in terms of morphology. shows The OH profiles along the inner and outer slits (Figure27) indicate a little anticipation of the flame front with increasing the H_2 content, in agreement with the fact that increasing the H_2 content the laminar flame speed increases.

Figure 26. OH field for G20, G222, H2NG for 15% of nominal load.

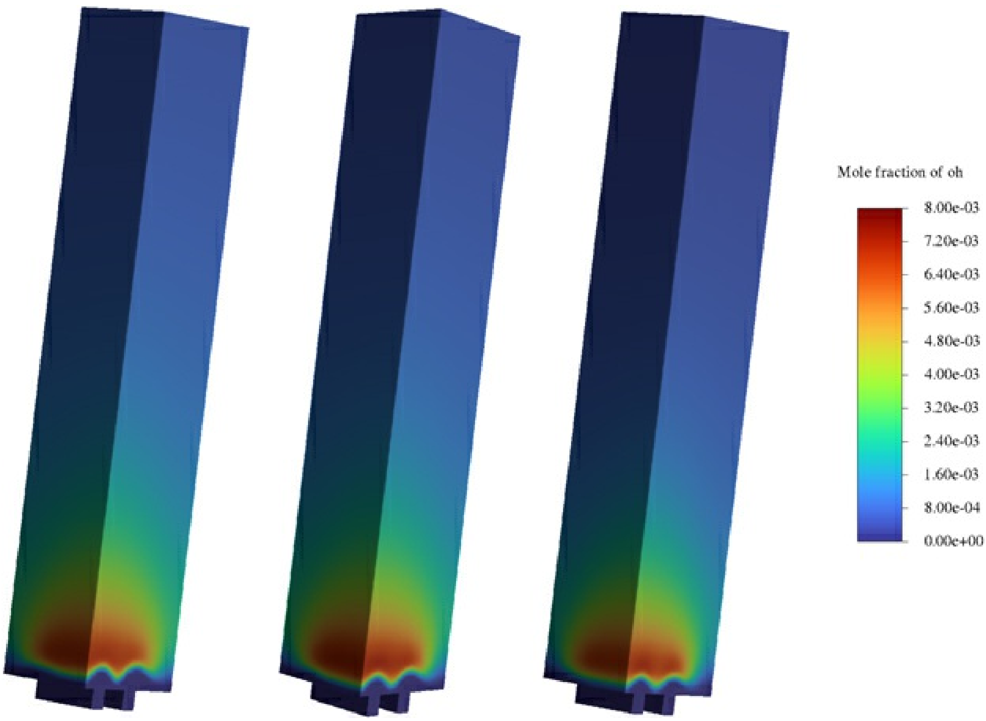

Figure 27. Profiles of OH mole fraction along X_1 (i.e. inner slit) and X_2 (i.e. outer slit) axes of B configuration at different H_2 content, i.e.: (a) inner slit; (b) outer slit.

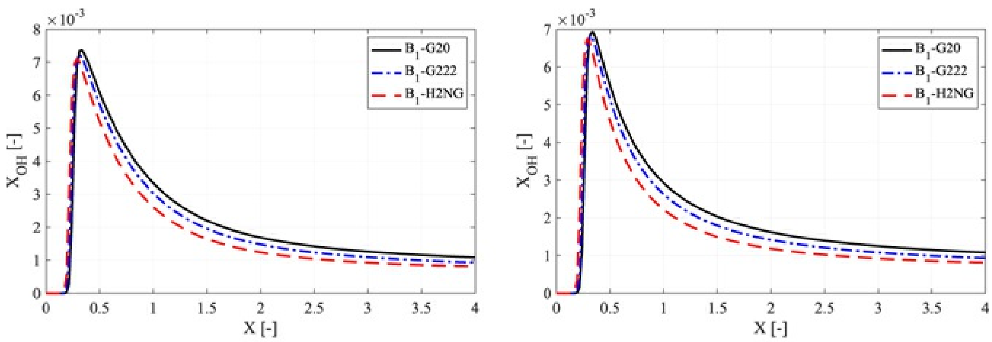

(a) (b)

4. Conclusions

The structure of methane-air flames issuing from groups of slits, mimicking two different pattern designs encountered in perforated burners of condensing boilers, is studied through 3-dimensional numerical simulations with a skeletal kinetic mechanism. In particular, the present work demonstrates that the slits, given their much larger dimensions than the holes, which have been extensively studied in the literature, show regime changes in terms of morphology, which may ultimately affect the burner performance also in terms of emissions.

For low inlet velocities, the flame issuing from a slit shows a flat region along the slit length, curved at the slit edge. Neighbour flames do not interact, appearing pretty similar to each other, even though the flames issuing from the outer slits are somewhat tilted with respect to the axis normal to the slit plane. This behaviour may be explained by the fact that the outer slit borders with burner hot walls have different extensions at the two lateral sides.

An increase in the issuing velocity leads to a completely different flame morphology. Firstly, the flame is no more flat, rather it assumes a conical shape along the slit length. Secondly, neighbour flames strongly interact with each other, leading to a strong effect of the slit pattern on the resulting flame structure. More specifically, flames issuing from a series of several slits merge generating a single long wedge-shaped flame, while flames issuing from a group of four slits produce just a single conical-shaped flame.

Hence the pattern plays a key role in the interaction and morphology of multiple flames. In particular, as the power and therefore the capacity of the condensing boiler increase, there are strong interactions between the adjacent flames which, by generating a single reactive front, increase the contribution of pollutants such as NOx by increasing the downstream temperature.

The availability of experimental NO emissions for one of the patterns, at different powers, supported the the numerical model, being CFD predictions well in agreement with the measurements. This result demonstrates the validity of the model in capturing the flame reaction zone which ultimately allows a good estimate of NOx. This knowledge may be used to improve both the burner design, in terms of geometries present in the diffusive zone, as well as the operation of the boiler, by for instance driving the setup of sensors for flame detection. Moreover, the availability of numerical models could help to understand the effect of upcoming variations in the fuel compositions. Indeed green energy vectors as hydrogen show much higher reactivity than methane, probably asking for a redesign of the burner which may benefit from the present modelling approach.

The structure of the flames generated by a portion of burner containing slits and holes is analysed and comparing with the configuration B we observe that profiles of temperature and OH almost overlaps, thus confirming the suitability of using a reduced domain including only the slits. A preliminary investigation on the effect of hydrogen addition for the B design is analysed where a H_2 content up to 50% is considered for the B1 case. As underlined in the section, the addition of H_2 to the gas mixture leads naturally to a higher air excess (see also [21, 46]), which partially limits the higher reactivity of hydrogen with respect to methane. Indeed the flame morphology is more less the same for both 0% and 50% hydrogen.

Acknowledgments

The authors thank Polidoro S.p.A. (Italy) for sharing the burners images.

Disclosure statement

No potential conflict of interest was reported by the author(s). **[Q3]**

ORCID

Rachele Lamioni http://orcid.org/0000-0002-7769-2493

Leonardo Tognotti http://orcid.org/0000-0001-5039-515X

Chiara Galletti http://orcid.org/0000-0003-1356-4246

References

1 **European Commission**, *A hydrogen strategy for a climate-neutral Europe*, 2020. Available at https://ec.europa.eu/energy/sites/ener/files.**[Q7]**

2 **G. Lo Basso , B. Nastasi, D. Astiaso Garcia, and F. Cumo**, *How to handle the hydrogen enriched natural gas blends in combustion efficiency measurement procedure of conventional and condensing boilers*, Energy 123 (2017), pp. 615–636.

3 **F. Schiro and A. Stoppato**, *Experimental investigation of emissions and flame stability for steel and metal fiber cylindrical premixed burners*, Combustion Sci. Technol. 191 (2019), pp. 453–471.

4 **S. Carpentier, P. Milin, N. Mostefaoui, P. Nitschke-Kowsky, J. Schweitzer Negar Sadegh, and O. Thibaut**, *Self-regulated gas boilers able to cope with gas quality variation state of the art and performances*, Report, 2018. Available at https://www.gerg.eu/wp-content/uploads/2019/10.

5 **D.T. Bălănescu and V.M. Homutescu**, *Experimental investigation on performance of a condensing boiler and economic evaluation in real operating conditions*, Appl. Thermal Eng. 143 (2018), pp. 48–58.

6 **X. Lin, H. Ma, C. Liu, J. Zhang, Y. Zhang, and Z. Miao**, *Experimental research on gas interchangeability indices for domestic fully premixed burners*, Fuel 233 (2018), pp. 695–703.

7 **R. Lamioni, P.E. Lapenna, L. Berger, K. Kleinheinz, A. Attili, H. Pitsch, and F. Creta**, *Pressure-induced hydrodynamic instability in premixed methane-air slot flames*, Combustion Sci. Technol. 192 (2020), pp. 1998–2009.

8 **T.H. Zhang, F.G. Liu, and X.Y. You**, *Optimization of gas mixing system of premixed burner based on cfd analysis*, Energy Conversion Manage. 85 (2014), pp. 131–139.

9 **D.F. Zhao, F.G. Liu, X.Y. You, R. Zhang, B.L. Zhang, and G.L. He**, *Optimization of a premixed cylindrical burner for low pollutant emission*, Energy Conversion Manage. 99 (2015), pp. 151–160.

10 **M.H. Saberi Moghaddam, M. Saei Moghaddam, and M. Khorramdel**, *Numerical study of geometric parameters effecting temperature and thermal efficiency in a premix multi-hole flat flame burner*, Energy 125 (2017), pp. 654–662.

11 **Z. Song, L. Wei, and Z. Wu**, *Effects of heat losses on flame shape and quenching of premixed flames in narrow channels*, Combustion Sci. Technol. 180 (2007), pp. 264–278.

12 **A. McIntosh and J.F. Clarke**, *Second order theory of unsteady burner-anchored flames with arbitrary lewis number*, Combustion Sci. Technol. 38 (1984), pp. 161–196.

13 **R. Rook, L. De Goey, L. Somers, K. Schreel, and R. Parchen**, *Response of burner-stabilized flat flames to acoustic perturbations*, Combustion Theory Modell. 6 (2002), p. 223.

14 **H.M. Altay, K.S. Kedia, R.L. Speth, and A.F. Ghoniem**, *Two-dimensional simulations of steady perforated-plate stabilized premixed flames*, Combustion Theory Modell. 14 (2010), pp. 125–154.

15 **H.d. Lange and L.d. Goey**, *Two-dimensional methane/air flame*, Combustion Sci. Technol. 92 (1993), pp. 423–427.

16 **K.S. Kedia and A.F. Ghoniem**, *Mechanisms of stabilization and blowoff of a premixed flame downstream of a heat-conducting perforated plate*, Combust. Flame. 159 (2012), pp. 1055–1069.

17 **E.V. Jithin, V.R. Kishore, and R.J. Varghese**, *Three-dimensional simulations of steady perforated-plate stabilized propane-air premixed flames*, Energy Fuels 28 (2014), pp. 5415–5425.

18 **S. Lee, J.M. Kim, S.M. Kum, and C.E. Lee**, *Suggestion on the simultaneous reduction method of co and nox in premixed flames for a compact heat exchanger*, Energy. Fuels. 24 (2010), pp. 821–827.

19 **J. Edacheri Veetil, B. Aravind, A. Mohammad, S. Kumar, and R.K. Velamati**, *Effect of hole pattern on the structure of small scale perorated plate burner flames*, Fuel 216 (2018), pp. 722–733.

20 **J. Hinrichs, D. Felsmann, S. Schweitzer-De Bortoli, H.J. Tomczak, and H. Pitsch**, *Numerical and experimental investigation of pollutant formation and emissions in a full-scale cylindrical heating unit of a condensing gas boiler*, Appl. Energy. 229 (2018), pp. 977–989.

21 **R. Lamioni, C. Bronzoni, M. Folli, L. Tognotti, and C. Galletti**, *Feeding h2-admixtures to domestic condensing boilers: Numerical simulations of combustion and pollutant formation in multi-hole burners*, Appl. Energy 309 (2022), p. 118379.

22 **S. Lee, S.M. Kum, and C.E. Lee**, *An experimental study of a cylindrical multi-hole premixed burner for the development of a condensing gas boiler*, Energy 36 (2011), pp. 4150–4157.

23 **S.S. Rashwan, A.H. Ibrahim, T.W. Abou-Arab, M.A. Nemitallah, and M.A. Habib**, *Experimental study of atmospheric partially premixed oxy-combustion flames anchored over a perforated plate burner*, Energy 122 (2017), pp. 159–167.

24 **H. Soltanian, M.Z. Targhi, and H. Pasdarshahri**, *Chemiluminescence usage in finding optimum operating range of multi-hole burners*, Energy 180 (2019), pp. 398–404.

25 **Y. Ding, D. Durox, N. Darabiha, and T. Schuller**, *Chemiluminescence of burner-stabilized premixed laminar flames*, Combustion Sci. Technol. 191 (2019), pp. 18–42.

26 **Y. Ding, D. Durox, N. Darabiha, and T. Schuller**, *Chemiluminescence based operating point control of domestic gas boilers with variable natural gas composition*, Appl. Therm. Eng. 149 (2019), pp. 1052–1060.

27 **R.M. Mallens, B.O. Loijenga, L.P. De Goey, and P.J. Sonnemans**, *Numerical and experimental study of lean M- and V-shaped flames*, Combustion Sci. Technol. 122 (1997), pp. 331–344.

28 **R. Mallens, H. de Lange, C.v. de VEN, and L. De Goey**, *Modeling of confined and unconfined laminar premixed flames on slit and tube burners*, Combustion Sci. Technol. 107 (1995), pp. 387–401.

29 **R.M.M. Mallens and L.P.H.D. Goey**, *Flash-back of laminar premixed methane/air flames on slitand tube burners*, Combustion Sci. Technol. 136 (1998), pp. 41–54.

30 **S. Parmentier, M. Braack, U. Riedel, and J. Warnatz**, *Modeling of combustion in a lamella burner*, Combustion Sci. Technol. 175 (2003), pp. 185–206.

31 **V.N. Kornilov, R. Rook, J.H. ten Thije Boonkkamp, and L.P. de Goey**, *Experimental and numerical investigation of the acoustic response of multi-slit Bunsen burners*, Combust. Flame. 156 (2009), pp. 1957–1970.

32 **T. Steinbacher, A. Albayrak, A. Ghani, and W. Polifke**, *Consequences of flame geometry for the acoustic response of premixed flames*, Combust. Flame. 199 (2019), pp. 411–428.

33 **R. Bilger, S. Stårner, and R. Kee**, *On reduced mechanisms for methane-air combustion in nonpremixed flames*, Combust. Flame. 80 (1990), pp. 135–149.

34 **P. Cheng**, *Two-dimensional radiating gas flow by a moment method*, AIAA J. 2 (1964), pp. 1662–1664.

35 **R. Siegel and J.R. Howell**, Thermal Radiation Heat Transfer, Hemisphere Pub, Corp., Washington, DC, 1992.

36 **T.F. Smith, Z.F. Shen, and J.N. Friedman**, *Evaluation of coefficients for the weighted sum of gray gases model*, J. Heat. Transfer. 104 (1982), pp. 602–608.

37 **A. Fluent**, *12.0 User's Guide*, Ansys Inc. 6, 2009.**[Q8]**

38 **G. De Soete**, *Overall reaction rates of no and n2 formation from fuel nitrogen*, Symposium (International) on Combustion 15 (1975), pp. 1093–1102. Fifteenth Symposium (International) on Combustion.

39 **P. Malte and D. Pratt**, *Measurement of atomic oxygen and nitrogen oxides in jet-stirred combustion*, Symposium (International) on Combustion 15 (1975), pp. 1061–1070. Fifteenth Symposium (International) on Combustion.

40 **M. Najarnikoo, M.Z. Targhi, and H. Pasdarshahri**, *Experimental study on the flame stability and color characterization of cylindrical premixed perforated burner of condensing boiler by image processing method*, Energy 189 (2019), p. 116130.

41 **A. Cuoci, A. Frassoldati, T. Faravelli, and E. Ranzi**, *Opensmoke++: An object-oriented framework for the numerical modeling of reactive systems with detailed kinetic mechanisms*, Comput. Phys. Commun. 192 (2015), pp. 237–264.

42 **T. Poinsot and D. Veynante**, Theoretical and numerical combustion, RT Edwards, Inc., 2005.**[Q9]**

43 **I. Ansys**, *Cfd, ICEM CFD Theory Guide*, Ansys Inc., 2015.**[Q10]**

44 **W. Francis and M.C. Peters**, *Data sheet no. 117 – fuel gas burners*, in *Fuels and Fuel Technology*, 2nd ed., W. Francis and M.C. Peters, eds., Pergamon, 1980, pp. 399–405.**[Q11]**

45 **D.M. Valiev, V. Akkerman, M. Kuznetsov, L.E. Eriksson, C.K. Law, and V. Bychkov**, *Influence of gas compression on flame acceleration in the early stage of burning in tubes*, Combust. Flame. 160 (2013), pp. 97–111.

46 **H. de Vries, A.V. Mokhov, and H.B. Levinsky**, *The impact of natural gas/hydrogen mixtures on the performance of end-use equipment: Interchangeability analysis for domestic appliances*, Appl. Energy. 208 (2017), pp. 1007–1019.